Quaternary Science Reviews 86 (2014) 144–157

Contents lists available at ScienceDirect

Quaternary Science Reviews

journal homepage: www.elsevier.com/locate/quascirev

Rock-slope failure following Late Pleistocene deglaciation on tectonically stable mountainous terrain

Colin K. Ballantyne [a,*], Graeme F. Sandeman [a], John O. Stone [b], Peter Wilson [c]

[a] School of Geography and Geosciences, University of St Andrews, Fife KY16 9AL, Scotland, UK
[b] Department of Earth and Space Sciences and Quaternary Research Center, University of Washington, Seattle, WA 98195-01310, USA
[c] School of Environmental Sciences, University of Ulster, Coleraine, UK

ARTICLE INFO

Article history:
Received 2 August 2013
Received in revised form
16 December 2013
Accepted 20 December 2013
Available online 21 January 2014

Keywords:
Rock-slope failure
Paraglacial
Stress-release
Palaeoseismicity
Cosmogenic isotopes

ABSTRACT

The ages of 31 postglacial rock-slope failures (RSFs) in Scotland and NW Ireland, derived from 89 cosmogenic isotope exposure ages, are employed to analyse the temporal pattern of failure and its relationship to the timing of deglaciation, rates of glacio-isostatic crustal uplift and periods of rapid climate change. RSF ages span almost the whole period since ice-sheet retreat, from 18.2 ± 1.2 ka to 1.7 ± 0.2 ka, or from 17.1 ± 1.0 ka to 1.5 ± 0.1 ka, depending on the production rate used in ^{10}Be age calculation, but catastrophic failure of rock slopes was ~4.6 times more frequent prior to ~11.7 ka than during the Holocene. 95% of dated RSFs at sites deglaciated during retreat of the last ice sheet occurred within ~5400 years after deglaciation, with peak RSF activity 1600–1700 years after deglaciation. This time lag is inferred to represent (1) stress release initiated by deglacial unloading, leading to (2) time-dependent rock mass strength degradation through progressive failure plane development, and ultimately (3) to either spontaneous kinematic release or failure triggered by some extrinsic mechanism. By contrast, 11 dated RSFs at sites reoccupied by glacier ice during the Younger Dryas Stade (YDS) of ~12.9–11.7 ka exhibit no clear temporal pattern, suggesting that glacial reoccupance during the YDS was ineffective in preconditioning a renewed cycle of enhanced RSF activity. Comparison of timing of individual RSFs with that of deglaciation and rapid warming events at ~14.7 ka and ~11.7 ka suggests that glacial debuttressing, enhanced joint water pressures during deglaciation and thaw of permafrost ice in rock joints could have triggered failure in only a small number of cases. Conversely, the timing of maximum RSF activity following ice-sheet deglaciation corresponds broadly with maximum rates of glacio-isostatic crustal uplift, suggesting that the two are linked by enhanced seismic activity. A seismic failure trigger is consistent with full-slope failure at all sites where failure planes are clearly defined. Our results indicate that numerous RSFs must have occurred in areas that were reoccupied by glacier ice during the YDS, but have not been identified because runout debris was removed by YDS glaciers. More generally, they provide the first reliably-dated body of evidence to support the view that retreat of the last ice sheets in tectonically-stable mountainous terrain initiated a period of enhanced rock slope failure due to deglacial unloading and probably Lateglacial seismic activity, implying that most undated RSFs in such areas are probably of Lateglacial or very early Holocene age. They also demonstrate, however, that a low frequency of RSF activity extended throughout the Holocene.

1. Introduction

Many formerly-glaciated mountain environments are characterized by a high spatial density of large-scale postglacial rock-slope failures (RSFs) in the form of major rockfalls, rockslides, rock avalanches or deep-seated gravitational slope deformations. Such RSFs are often described as *paraglacial*, implying that failure was conditioned by the preceding episode of glaciation and deglaciation (Ballantyne, 2002; Wilson, 2009; Kellerer-Pirklbauer et al., 2010; McColl, 2012). Several authors have inferred a causal connection between deglaciation of steep rockwalls and subsequent rock-slope failure, with regard to both recent retreat of mountain glaciers (e.g. Evans and Clague, 1994; Holm et al., 2004; Arsenault and Meigs, 2005; Allen et al., 2010) and shrinkage of Late Pleistocene ice sheets (e.g. Abele, 1997; Soldati et al., 2004; Blikra et al., 2006; Longva et al., 2009; Mercier et al., 2013; Cossart et al., 2013a). Proposed explanations for this association include stress-release fracturing, uplift and dilation of rock masses,

* Corresponding author. Tel.: +44 0 1334 463907; fax: +44 0 1334 463949.
E-mail address: ckb@st-andrews.ac.uk (C.K. Ballantyne).

0277-3791/$ – see front matter © 2014 Elsevier Ltd. All rights reserved.
http://dx.doi.org/10.1016/j.quascirev.2013.12.021

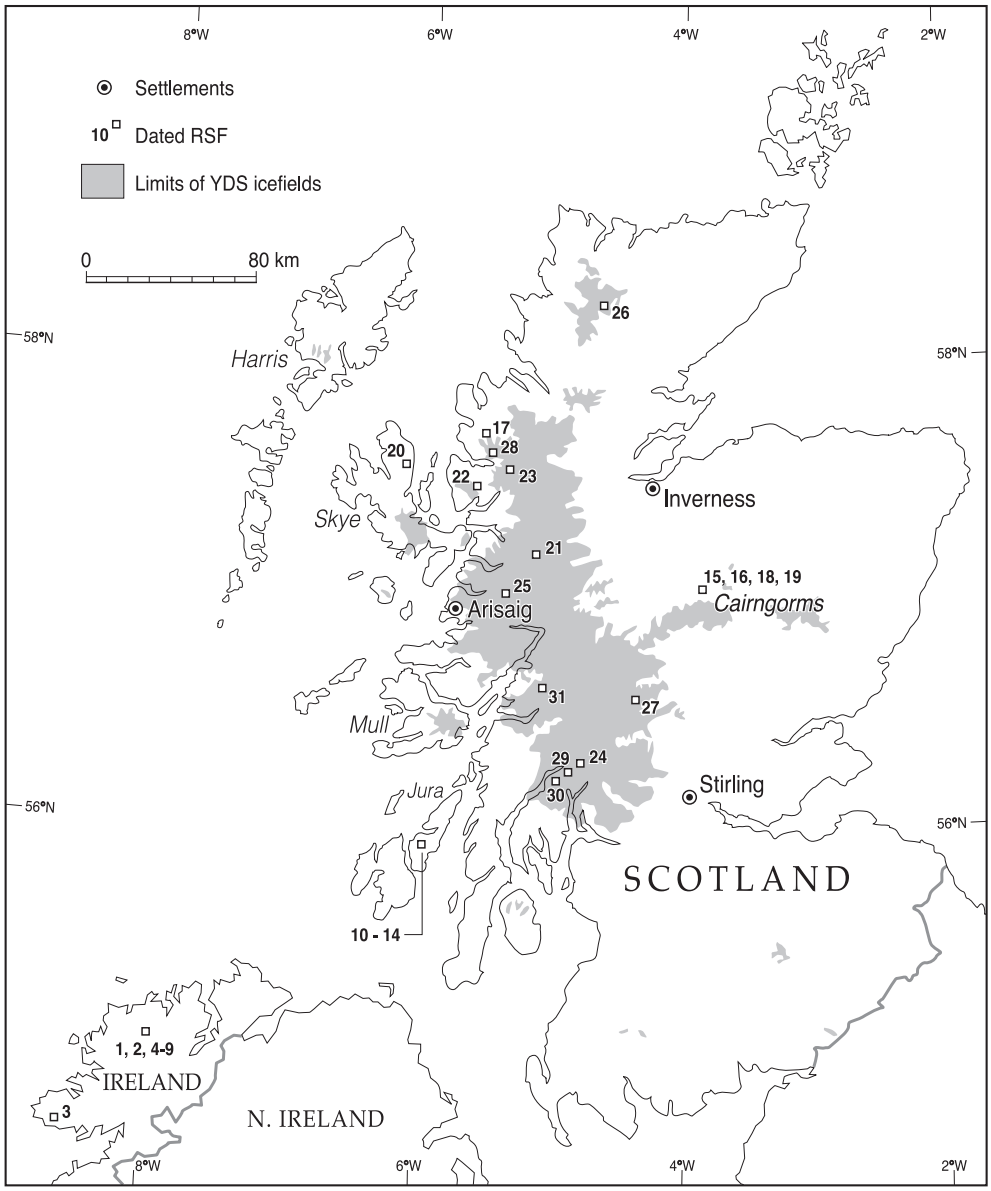

Fig. 1. Location of RSF sites (numbering as in Table 1), showing the extent of Younger Dryas icefields and other locations mentioned in the text.

debuttressing (removal of supporting glacier ice from unstable rockwalls), freeze-thaw activity, thaw of permafrost ice in ice-bonded joint networks, enhanced joint-water pressures during deglaciation and seismic activity (Prager et al., 2008; McColl, 2012).

In the case of RSFs following Late Pleistocene or early Holocene deglaciation, assessment of the manner in which deglaciation has affected rock-mass stability has been impeded by limited data on the timing of postglacial failures. Over the past two decades, however, surface exposure dating using cosmogenic isotopes (^{3}He, ^{10}Be, ^{21}Ne and ^{36}Cl) has been employed to establish the age of numerous individual postglacial RSFs, particularly in tectonically-active mountain belts such as the Alps (Bigot-Cormier et al., 2005; Van Husen et al., 2007; Hormes et al., 2008; El Bedoui et al., 2009; Hippolyte et al., 2009; Ivy-Ochs et al., 2009; Prager et al., 2009; Sanchez et al., 2010), Himalaya (Mitchell et al., 2007; Dortch et al., 2009), Andes (Hermanns et al., 2001, 2004; Fauqué et al., 2009; Welkner et al., 2010) and Karakoram (Seong et al., 2009; Shroder et al., 2011). Most of these studies, however, involve the dating of a single RSF or small number of RSFs, so the regional temporal pattern of RSF activity since deglaciation cannot be assessed. Moreover, almost all exposure-dated RSFs are located in tectonically-active mountain belts. In such areas earthquakes caused by postglacial fault movements due to tectonically-driven uplift or regional crustal stresses may trigger major RSFs, so that RSF ages may be largely independent of the timing of Late Pleistocene deglaciation (e.g. Hewitt et al., 2008, 2011; Antinao and Gosse, 2009; Sanchez et al., 2010; Stock and Uhrhammer, 2010; Hermanns and Niedermann, 2011; Penna et al., 2011).

Numerous postglacial RSFs are also present in mountainous parts of seismically-quiescent intraplate terrains, such as Scandinavia and much of the British Isles, that were completely buried under Late Pleistocene ice sheets. The Scottish Highlands, for example, are estimated to contain over 550 postglacial RSFs, including 140 with areas exceeding 0.25 km^2 (Jarman, 2006, 2007). For such areas, several authors have championed the idea that active faulting driven by glacio-isostatic rebound produced large magnitude ($M > 6.0$) earthquakes following ice-sheet shrinkage, with progressive reduction in seismic activity during the Holocene

as the rate of uplift slowed (Davenport et al., 1989; Gregerson and Basham, 1989; Ringrose, 1989a; Dehls et al., 2000; Morner, 2004, 2005; Lagerbäck and Sundh, 2008). One implication of this view is that many RSFs in mountain areas presently characterized by low-level seismic activity may have been released by earthquakes in the aftermath of ice sheet retreat, with diminishing RSF activity thereafter. Some support for this view is provided by research on the stratigraphy of inferred rock avalanche deposits in Norwegian fjords: Blikra et al. (2006) detected a peak of RSF activity during deglaciation and Longva et al. (2009) inferred that ~89% of the volume of postglacial rock avalanche deposits in Storfjorden (western Norway) represents deposition during ice-sheet deglaciation (~14.7–11.7 ka), though the frequency of rock avalanches apparently peaked in the early Holocene (~11.7–10.0 ka). Similarly, Strasser et al. (2013) concluded that a high frequency of Lateglacial (~16.7–11.6 ka) landslide events represented stratigraphically in lacustrine sediment sequences in Central Switzerland represents enhanced seismic activity attributable to glacio-isostatic crustal movements.

Over the past 15 years we have amassed a database of 31 dated rock-slope failures in the Scottish Highlands, Inner Hebrides and NW Ireland (Fig. 1) based on a total of 89 ^{10}Be or ^{36}Cl exposure ages obtained on runout debris (Ballantyne et al., 1998, 2009a, 2013a, 2013b; Ballantyne and Stone, 2004, 2009, 2013). The aim of this paper is to synthesise all the dating evidence from this research to characterize the timing of postglacial RSFs in this tectonically-stable region and to examine the implications in terms of the long-term causes and short-term triggers of failure. More specifically, we employ this unique dataset to test various hypotheses concerning the relationship between the timing of deglaciation and RSF response, namely: (1) that failure represents a rapid, immediate response to deglaciation; (2) that RSF activity was focused within a few millennia during the Lateglacial and Early Holocene, as suggested by several previous studies (Blikra et al., 2006; Prager et al., 2008; Fauqué et al., 2009; Longva et al., 2009); (3) that the timing of failure involves elements of both rapid and delayed response to deglaciation, as proposed by Ballantyne and Stone (2013); and (4) that the timing of failure extended throughout the postglacial period, with limited temporal clustering, as suggested by an inventory of dated RSFs compiled by Prager et al. (2008) for the Austrian Tyrol.

2. Study areas

The mountains of the Scottish Highlands, the Inner Hebrides and NW Ireland are largely underlain by metasedimentary rocks or sandstones of Neoproterozoic age, or by granitic rocks of Devonian age. Of the 31 dated RSFs, all those in NW Ireland and on the Isle of Jura (1–14 in Table 1 and Fig. 1) are seated on massive, well-bedded quartzites of Dalradian age, though most exhibit no relationship between the locus of failure and local dip of the bedding planes (Ballantyne et al., 2013b). Of the dated RSFs in the Scottish Highlands, four are located on granite (15, 16, 18, 19), two on Torridon sandstone (17, 28), and most of the remainder on metamorphic rocks (pelitic, semi-pelitic or psammitic schists, quartzite or granulite), though one (31) occurred within rhyolitic ignimbrite. The

Table 1
RSF ages.

Rock slope failure	Lithology	LL LPR		NWH11.6 LPR	
		Exposure age (ka)	Total uncertainty (ka)	Exposure age (ka)	Total uncertainty (ka)
NW Ireland RSFs					
1. Errigal-4	Quartzite	17.71	0.89	16.56	0.68
2. Aghla More East	Quartzite	17.18	0.90	16.06	0.69
3. Slieve League	Quartzite	17.04	0.91	15.94	0.71
4. Errigal-1	Quartzite	16.04	0.86	15.00	0.66
5. Muckish	Quartzite	16.02	0.86	14.99	0.67
6. Ardloughnabrackbaddy	Quartzite	15.52	0.83	14.52	0.64
7. Aghla Beg	Quartzite	15.44	0.83	14.45	0.65
8. Aghla More West	Quartzite	13.00	0.68	12.16	0.52
9. Mackoght	Quartzite	12.50	0.66	11.69	0.51
Jura RSFs					
10. Beinn a'Chaolais West	Quartzite	15.37	0.92	14.37	0.74
11. Beinn Shiantaidh	Quartzite	15.11	0.81	14.14	0.63
12. Beinn a'Chaolais South	Quartzite	14.66	0.75	13.70	0.57
13. Beinn an Oir East	Quartzite	14.38	0.88	13.45	0.72
14. Beinn a'Chaolais East	Quartzite	13.67	0.73	12.78	0.57
Scottish Highlands and Skye (outside Younger Dryas glacier limit)					
15. Strath Nethy	Granite	18.15	1.16	17.06	0.96
16. Lairig Ghru	Granite	17.17	1.03	16.04	0.84
17. Baosbheinn	Sandstone	14.99	0.75	14.01	0.56
18. Coire Beanaidh	Granite	14.26	0.86	13.32	0.73
19. Coire Etchachan	Granite	13.64	0.82	12.76	0.67
20. The Storr (Skye)	Basalt	6.08	0.49	(^{36}Cl exposure age)	
Scottish Highlands (inside Younger Dryas glacier limit)					
21. Carn Ghluasaid	Schist	12.68	0.68	11.86	0.53
22. Coire nan Arr[a]	Sandstone	12.46	0.60	11.69	0.44
23. Maol Chean-dearg[a]	Quartzite	12.42	0.58	11.62	0.42
24. Beinn an Lochain	Schist	11.71	0.58	10.95	0.43
25. Druim nan Uadhag	Schist	9.91	0.52	9.27	0.40
26. Carn nan Gillian	Granulite	7.87	0.40	7.36	0.53
27. Carn Ban	Schist	4.86	0.33	4.55	0.28
28. Beinn Alligin	Sandstone	4.42	0.32	4.14	0.27
29. Hell's Glen	Schist	3.82	0.22	3.52	0.17
30. Mullach Coir a'Chuir	Schist	1.65	0.15	1.54	0.13
31. Coire Gabhail	Ignimbrite	1.68	0.22	(^{36}Cl exposure age)	

[a] RSF runout on to Younger Dryas Stadial glacier.

Fig. 2. (a) Slieve League RSF (3) NW Ireland. (b) Runout from Errigal 1 RSF (4), NW Ireland, photographed from the summit ridge of Errigal Mountain. (c) Beinn Shiantaidh RSF (11), Isle of Jura. (d) Hell's Glen RSF (29), SW Scottish Highlands. (e) Beinn Alligin RSF (28), NW Scottish Highlands. (f) Maol Chean-dearg RSF (23), NW Scottish Highlands; quartzite runout debris has been transported away from the failure site by residual glacier ice near the end of the Younger Dryas Stade.

single dated RSF on the Isle of Skye (20) represents failure of stacked basalt lavas seated on underlying Jurassic shale. Summit altitudes at the dated RSF sites range from ~550 m in NW Ireland to ~1150 m in the Cairngorm Mountains in the north-eastern Highlands. Vertical travel distances of individual dated RSFs generally range from ~100 m to ~400 m, except in the case of the Beinn Alligin rock avalanche, where runout debris from a 500 m high failure plane extends a further 1.25 km downvalley, giving a total vertical descent of ~650 m (Ballantyne and Stone, 2004).

During the last glacial maximum (~26–21 ka) the last British-Irish ice sheet covered all mountain summits in Scotland and NW Ireland, extended to the Atlantic shelf edge in the west and was confluent with the Fennoscandian Ice sheet in the North Sea Basin (Bradwell et al., 2008; Hubbard et al., 2009; Clark et al., 2012; Fabel et al., 2012; Ó Cofaigh et al., 2012). By ~19 ka the ice sheet margin had retreated to the present coast in NW Ireland (Clark et al., 2009), and by ~15 ka the ice margin was located along the western seaboard of Scotland, extensive areas of the eastern Highlands were ice free, and the summits of mountains in the Scottish Highlands had emerged from the ice sheet as nunataks (Phillips et al., 2008; Ballantyne, 2010; Ballantyne and Stone, 2012; Fabel et al., 2012). Following rapid warming at the onset of the Lateglacial Interstade at ~14.7 ka, when mean July temperatures in Scotland rose by ~6 °C (Brooks and Birks, 2000; Brooks et al., 2012), glacier ice completely disappeared from all mountain area of the British Isles, or survived only in favourable locations such as cirques or high plateaus in the northern and western Highlands (Finlayson et al., 2011; Ballantyne and Stone, 2012). Rapid temperature decline at the onset of the ensuing Younger Dryas Stade (YDS) of ~12.9–11.7 ka resulted in renewed expansion of glacier ice, which formed a major ice cap or icefield in the western Highlands, several smaller peripheral icefields and numerous independent cirque and valley glaciers (Golledge, 2010, Fig. 1). Postglacial RSFs in NW Ireland and in Scotland outside the limits of YDS glaciation may therefore have occurred at any time since local deglaciation as the British-Irish Ice Sheet retreated (19–14 ka), whereas postglacial RSFs inside the YDS glacier limits must have occurred since YDS glacier retreat, which occurred within the period 12.5–11.5 ka (Golledge et al., 2008; Golledge, 2010; Ballantyne, 2012). Glacier ice has been absent from the British Isles throughout the Holocene. Permafrost is known to have developed down to sea level in the wake of the retreating ice sheet prior to warming at ~14.7 ka, and again during the YDS (Ballantyne and Harris, 1994). It is possible that residual permafrost survived under high ground during the intervening

Lateglacial Interstade (~14.7–12.9 ka), but evidence for this is lacking.

NW Ireland and Scotland occupy intraplate terrain of relative tectonic stability. The region is presently characterized by low magnitude ($M_L < 4$) seismic activity focused mainly in the western Highlands (Musson, 2007), possibly reflecting interaction of NW–NNW directed tectonic stress and residual glacio-isostatic rebound (Firth and Stewart, 2000; Muir-Wood, 2000).

3. RSF characteristics and sampling

The characteristics of the 31 dated RSFs and details of sampling are summarised in Ballantyne and Stone (2013), and Ballantyne et al. (2013a, 2013b). Almost all sampled RSFs represent catastrophic translational rockslides or rock avalanches involving kinematic release of 0.2–10.0 Mt of rock and runout of coarse bouldery debris (Fig. 2), though failure at The Storr on Skye (20) took the form of foundering of basalt lavas on underlying shale in the form of a lateral block glide. Although deep-seated gravitational slope deformations are common on metamorphic rocks in the Scottish Highlands (Jarman, 2006, 2007), these lack runout debris and hence were not included in our dating campaign because of the difficulty of finding outcrops suitable for exposure dating.

In all cases but one, samples for exposure dating were chiseled from near-horizontal surfaces of large boulders in the RSF runout zones; the exception was the RSF at The Storr (20), where we sampled the tops of shattered bedrock pinnacles. Sampling was focused wherever possible on the distal part of the runout zone to reduce the possibility of sampling boulders emplaced by rockfall events subsequent to the main failure event. In two cases (22 and 23) we sampled boulders from RSF runout debris that had been deposited on, and transported downslope by, residual YDS glaciers (Fig. 2f), implying that these RSFs occurred towards the end of the YDS (Ballantyne and Stone, 2013). At all other sites there is no evidence for displacement of RSF debris by glacier ice, indicating that failure occurred after final deglaciation of these sites.

For four sites (20, 21, 24 and 25 in Fig. 1 and Table 1), two samples were submitted for analysis; for all other sites three samples were submitted. At all but two sites, quartz-rich lithologies were submitted for analysis of cosmogenic ^{10}Be in quartz, the exceptions being the two RSFs in igneous rocks (20 and 31) which were analysed for whole-rock cosmogenic ^{36}Cl. Full details of the analytical data and procedures are given in Ballantyne and Stone (2013) and Ballantyne et al. (2013a, 2013b).

4. Calibration of RSF ages

Calculation of the ^{36}Cl exposure ages obtained for RSFs 20 and 31 is described in Ballantyne and Stone (2013). ^{10}Be exposure ages for all other sites were calculated using the CRONUS-Earth online calculator (Balco et al., 2008) and calibrated (or recalibrated) using two local ^{10}Be production rates (LPRs) to minimise scaling uncertainty (Balco, 2011). The first, the Loch Lomond LPR (LL LPR) is based on ^{10}Be concentration in samples from boulders on an independently-dated YDS terminal moraine (Fabel et al., 2012), and implies a reference production rate (Lm scaling) of 3.92 ± 0.18 atoms g^{-1} a^{-1}, similar to the Arctic ^{10}Be production rate (3.96 ± 0.15 atoms g^{-1} a^{-1}) of Young et al. (2013). The second is the NWH11.6 LPR, which is based on ^{10}Be concentration on samples from bedrock surfaces and glacially-deposited boulders inside the limits of small YDS glaciers in the NW Highlands (Ballantyne and Stone, 2012). An assigned deglacial age of 11.6 ± 0.3 ka, based on the timing of rapid summer warming at the YDS-Holocene climatic transition (Brooks and Birks, 2000; Brooks et al., 2012), yields a reference ^{10}Be production rate (Lm scaling) of 4.20 ± 0.14 atoms g^{-1} a^{-1} for an assumed surface erosion rate of 1 mm ka^{-1}, similar to that of 4.26 atoms g^{-1} a^{-1} calculated by Balco et al. (2009) for Lateglacial sites in northeastern North America. As the small glaciers at the sites from which the NWH11.6 production-rate calibration samples were obtained may have retreated before 11.6 ka (Golledge et al., 2008; Ballantyne, 2012), this production rate should be regarded as maximal, producing the youngest possible ages for our RSF samples. The two LPRs thus effectively bracket the range of possible exposure ages (Fabel et al., 2012). The NHW11.6 LPR produces exposure ages 6.8–7.0% lower than the LL LPR, or roughly 1000 years younger for LL LPR ages of 14–15 ka. We report ages using the time-dependent Lm scaling of the CRONUS-Earth calculator (Lal, 1991; Stone, 2000), which is widely employed in studies of deglaciation chronology within the British Isles. Other scaling schemes available using the CRONUS-Earth calculator produce ages up to 1.5% older or 0.5% younger. We assume a surface erosion rate (ε) of 1 mm ka^{-1} for all samples. Although this is a reasonable assumption for crystalline rocks (Ballantyne, 2010), it probably overestimates erosion rates for some lithologies, such as quartzite, and may underestimate it for others, such as sandstone. However, assumption of $\varepsilon = 0$ reduces our reported ages by only ~1% and assumption of $\varepsilon = 2$ mm ka^{-1} increases reported ages by a similar margin, with negligible effect on the temporal pattern of RSF ages reported here. Moreover, use of a particular LPR, scaling scheme or erosion rate has negligible effect on analysis of RSF ages relative to local deglaciation ages (which were also derived from cosmogenic isotope exposure ages), as all ages are affected proportionately. Below we cite ages calibrated using LL LPR first, followed by ages calibrated using NWH11.6 LPR in brackets. Uncertainties are cited as external (total) dating uncertainties at ± 1σ.

To derive a best-estimate age for each of the 31 dated RSFs we first excluded 'outlier' ages that differ from others obtained from the same site at $p < 0.05$, to produce pairs or triplets of statistically-indistinguishable individual ages. We then calculated the uncertainty-weighted mean age for each RSF from the remaining ages. Ten of our weighted mean ages (Table 1) are based on three consistent individual ages and 19 on two consistent individual ages. The age of two sites (10 and 13) are based on the single oldest postglacial age obtained at these sites, where significantly younger ages probably reflect sampling from boulders emplaced by later rockfall or debris-flow events (Ballantyne et al., 2013a).

5. Timing of deglaciation

The timing of deglaciation at RSF sites outside the limit of YDS glaciation in the Scottish Highlands and Skye was determined from independent local deglaciation chronologies based on ^{10}Be or (in one case) ^{36}Cl exposure age dating of bedrock surfaces or boulders on moraines (Stone et al., 1998; Everest and Kubik, 2006; Ballantyne et al., 2009b; Ballantyne, 2010; Ballantyne and Stone, 2012), recalculated where appropriate using LL LPR and NWH11.6 LPR. For sites in the Scottish Highlands that were reoccupied by glacier ice during the YDS (~12.9–11.7 ka) we assume a deglaciation age of 11.6 ± 0.3 ka, consistent with very rapid warming after 11.7 ka (Brooks and Birks, 2000; Hubbard et al., 2009; Brooks et al., 2012) and ^{14}C-based evidence that some YDS were still advancing to their maximum extent as late as 12.0–11.7 ka (Macleod et al., 2011). It is probable, however, that some YDS glaciers reached their maximum extent and began to retreat a few centuries prior to 11.6 ka (Golledge et al., 2008; Ballantyne, 2012), implying that the time elapsed between deglaciation and RSF occurrence should be regarded as minimal for RSFs sampled inside the limits of YDS glaciation. For eight RSFs in NW Ireland (1,2 and 4–9) we derive deglaciation age from the weighted mean (17.4 ± 0.9 ka (16.3 ± 0.7 ka)) of three ^{10}Be exposure ages for bedrock samples

from an adjacent col (Ballantyne et al., 2013b), and deglaciation age for the Slieve League RSF (3) is approximated by a ^{10}Be exposure age of 19.3 ± 1.0 ka (18.1 ± 0.8 ka) reported by Ballantyne et al. (2007) for a nearby site. The timing of deglaciation for the Jura RSFs is represented by the mean ^{10}Be exposure age of 16.8 ± 0.9 ka (15.8 ± 0.5 ka) obtained for two samples from a nearby moraine (Ballantyne et al., 2013a).

6. RSF ages

The ages of the 31 dated RSFs are summarised in Table 1 and plotted cumulatively in Fig. 3. The data demonstrate that RSFs have occurred throughout almost the entire postglacial period, from 18.2 ± 1.2 ka (17.1 ± 1.0 ka) to 1.7 ± 0.2 ka (1.5 ± 0.1 ka). They also suggest, however, that the frequency of RSFs was not constant throughout this time interval. A remarkable feature of Fig. 3 is the inflection that occurs at ~11.7 ka, which coincides with the end of the YDS and beginning of the Holocene. Before ~11.7 ka the cumulated number of RSFs (N) increases steeply with age (A, expressed in ka) as summarised by the regression equations:

$$N = 3.607(A - 11.7) + 8.694 \quad \left(n = 22;\ r^2 = 0.985\right) \tag{1}$$

for RSF ages calculated using LL LPR, and

$$N = 3.846(A - 11.7) + 11.626 \quad \left(n = 22; r^2 = 0.984\right) \tag{2}$$

for ages calculating using NWH11.6 LPR. The reciprocal of the slope of the regression lines indicates that the sampled RSFs with pre-Holocene ages occurred on average every ~280 years (equation (1)) or ~260 years (equation (2)). The periodicity of all 22 Late-glacial (i.e. pre-Holocene) RSFs is indistinguishable from a null hypothesis of constant periodicity generated by assuming one sampled failure per 280 years (LL LPR) or one failure per 260 years (NWH11.6 LPR), tested using a one-sample χ^2 test at $p < 0.001$.

Regression of the cumulated number of RSFs against age for the nine Holocene RSFs yields:

$$N = 0.769A + 0.540 \quad \left(n = 9; r^2 = 0.958\right) \tag{3}$$

for RSF ages calculated using LL LPR, and

$$N = 0.827A + 0.490 \quad \left(n = 9; r^2 = 0.966\right) \tag{4}$$

for ages calculated using NWH11.6 LPR. In this case the reciprocals of the slopes of these two regression lines imply respectively an average periodicity of one sampled RSF per 1300 years and one sampled RSF per 1200 years, and again the periodicity of RSF occurrence does not differ at $p < 0.005$ from a null hypothesis of constant periodicity. If our sample of ages is representative, these results imply (1) that the frequency of Lateglacial RSFs was roughly 4.6 times greater than that of Holocene RSFs, and (2) that there is no significant clustering of ages in either period.

7. Timing and periodicity of RSFs since deglaciation

The pattern of exposure ages alone, however, does not take into account differences in the timing of deglaciation at individual sites.

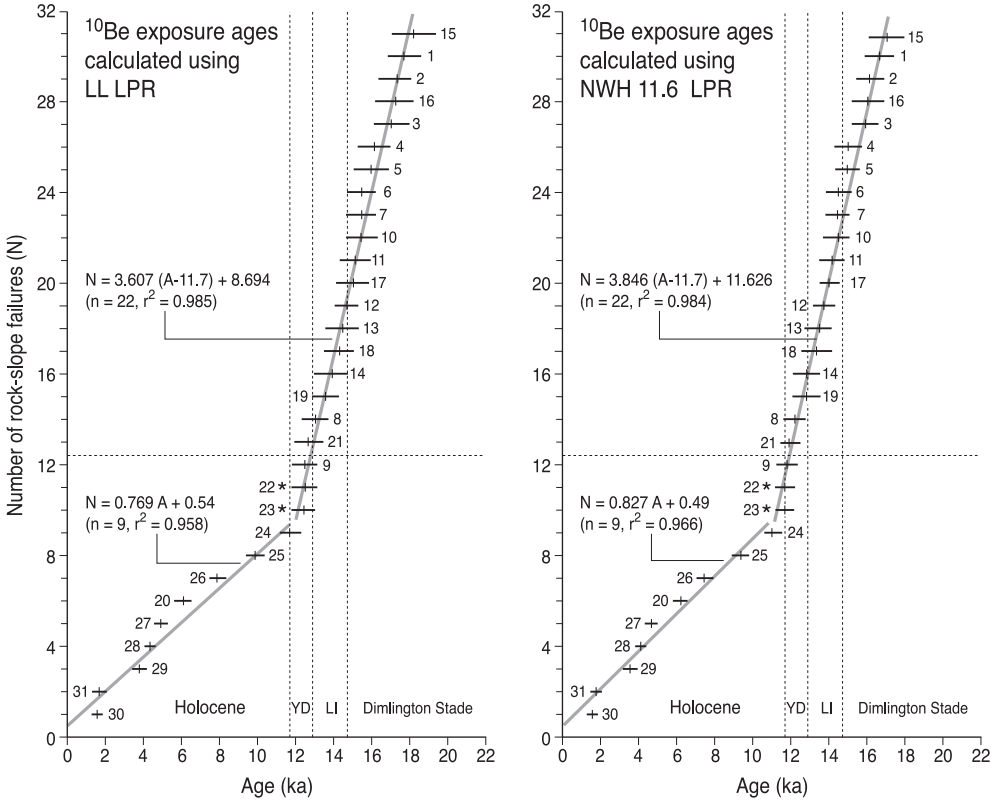

Fig. 3. Ages for all 31 dated RSFs, arranged by ascending age. Numbering of RSFs follows Table 1. Vertical dashes are uncertainty-weighted mean ages, and horizontal bars indicate ± 1σ total uncertainties. All ages above the horizontal dashed line represent sites deglaciated during ice-sheet retreat and not reoccupied by glacier ice during the Younger Dryas Stade. Ages below the horizontal dashed line represent sites reoccupied by glacier ice during the Younger Dryas Stade, except sites 9 and 20, which were deglaciated during ice-sheet retreat. Vertical dashed lines separate the Dimlington Stade (>14.7 ka), the Lateglacial Interstade (LI: 14.7–12.9 ka), the Younger Dryas Stade (YD: 12.9–11.7 ka) and the Holocene (<11.7 ka).

Fig. 4 depicts probability density distributions (PDDs) for all RSFs ($n = 31$), for all RSF sites deglaciated during retreat of the last ice sheet and not subsequently reoccupied by ice during the YDS ($n = 20$) and for all RSFs that were sampled inside the limits of YDS glaciation ($n = 11$), in all cases calculated as time elapsed since deglaciation (t) for each RSF site. Because the PDDs take into account both mean age and the associated $\pm 1\sigma$ uncertainties, the PDD curves extend to the left of $t = 0$, even though postglacial landslides cannot have occurred prior to deglaciation, except in the case of the two RSFs (22, 23) that occurred on to residual glacier ice at the end of the YDS. The weighted mean age obtained for four other RSFs (1, 15, 16 21) slightly exceeds the assumed deglaciation age for these sites, and for these sites $t = 0$ was assumed in generating the PDDs.

The plots for all RSFs (Fig. 4a and d) highlight a tendency for RSFs to be clustered within a few millennia following deglaciation, but with two modal values. The earlier mode peaks 100–300 years following deglaciation and represents a subset of nine (29%) 'rapid response' RSFs (1, 2, 15, 16, 17, 21, 22, 23, 24) whose weighted mean age is statistically indistinguishable from the timing of deglaciation; the age of all other RSFs is significantly younger than the timing of local deglaciation at $p < 0.05$. The second mode peaks ~1700 years after deglaciation. By calculating areas under the curves for the region $t > 0$, it is possible to retrodict probability of failure within given time periods: Fig. 4a (based on LL LPR ages) implies 70% probability of failure within 3000 years following deglaciation and 88% within 5000 years; the equivalent figures for Fig. 4d (based on NWH11.6 LPR ages) are 73% and 92%.

The most striking feature of Fig. 4 is the different pattern of response for sites deglaciated during retreat of the last ice sheet (Fig. 4b and e) and those deglaciated during retreat of YDS glaciers (Fig. 4c and f), particularly if the ages of the RSFs that occurred on to residual YDS glaciers (dashed lines) are excluded. The PDDs for the former peak 1600–1700 years after deglaciation then decline rapidly, and imply a 74% (78%) probability of failure within 3000 years following deglaciation and 93% (94%) within 5000 years after deglaciation. Of the 20 RSF sites deglaciated during retreat of the last ice sheet, only that at The Storr on Skye (20) failed more than ~5400 years after deglaciation. By contrast, RSFs sites deglaciated during retreat of YDS glaciers exhibit no clear temporal pattern, particularly if the sample is randomized by excluding failures on to the surfaces of residual YDS glaciers (dashed lines in Fig. 4c and f).

In terms of the four hypotheses outlined in the introduction there is only limited evidence for failure as a rapid, immediate response to deglaciation (less than 29% of sampled RSFs), but strong evidence for concentration of RSF activity within a few millennia following ice-sheet shrinkage (Fig. 4b and e) as suggested by previous studies in Scandinavia (Morner, 2004; Blikra et al., 2006; Longva et al., 2009) and Central Switzerland (Strasser et al., 2013). In general, the pattern of a combination of both rapid and delayed response identified by Ballantyne and Stone (2013) fits the combined data (Fig. 4a and d), though the initial 'rapid' response is more muted than their analysis suggested. The proposition that the timing of failure extends throughout the postglacial period without significant clustering is refuted by the full data set (Fig. 4a and d) and for sites deglaciated during ice-sheet shrinkage and not reoccupied by glacier ice during the YDs (Fig. 4b and d), but not for sites reoccupied by glacier ice during the YDS (Fig. 4c and f).

8. Causes of failure

Retrodiction of the factors responsible for preconditioning or triggering RSFs in formerly-glaciated mountains has focused on (1) paraglacial stress release and consequent fracture propagation associated with deglacial unloading of rock slopes and (2) the role of particular extrinsic mechanisms ('debuttressing', earthquakes, thaw of permafrost ice in joints, frost wedging and high joint-water pressures) in triggering failure of fractured rock masses (Braathen et al., 2004; Prager et al., 2008; McColl, 2012). The possible contribution of each of these mechanisms is considered below.

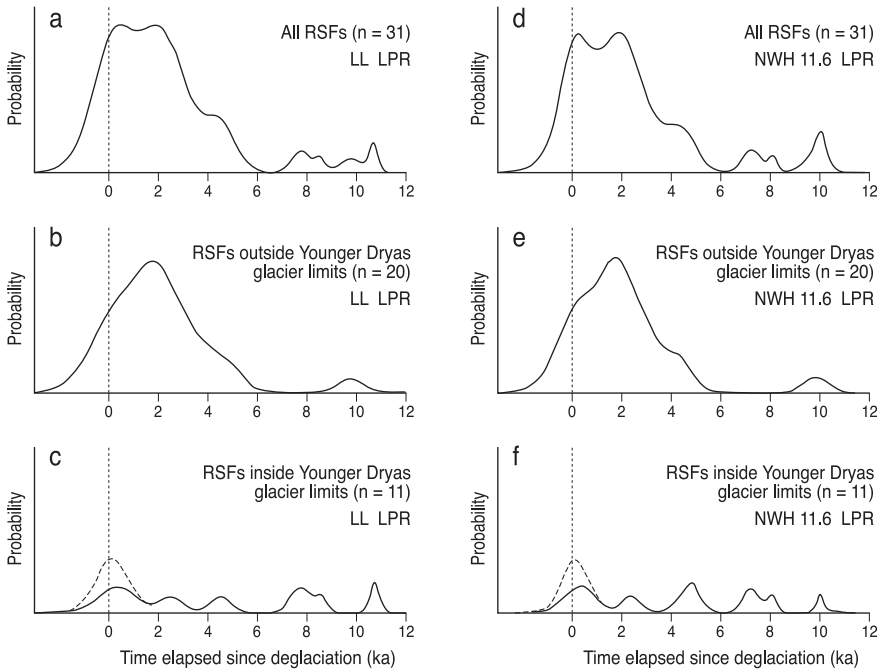

Fig. 4. Probability density distributions (PDDs) of RSF ages, calculated as time elapsed since deglaciation (vertical line; $t = 0$). (a–c): calculated using LL LPR; (d–f) calculated using NWH11.6 LPR. (a, d): all RSFs. (b, e): RSF sites deglaciated by retreat of the last ice sheet. (c, f): RSF sites reoccupied by glacier ice during the YDS; dashed line includes sites 22 and 23, where RSFs debris fell on to residual glaciers towards the end of the YDS.

8.1. Stress release

Paraglacial stress release is the development of tensile stresses within a rock mass as a result of deglacial unloading, and has been widely cited as a key factor in explaining postglacial RSFs (e.g. Soldati et al., 2004; Bigot-Cormier et al., 2005; Agliardi et al., 2009; Gugliemi and Cappa, 2010; Crosta et al., 2013) but the process is incompletely understood. Some authors have emphasized loading by glacier ice and subsequent unloading during deglaciation in altering the state of stress within valley-side slopes (e.g. Wyrwoll, 1977; Augustinus, 1995; Cossart et al., 2008, 2013a; Mercier et al., 2013). This model, however, disregards both the effects of topographically-induced stresses (Miller and Dunne, 1996; Molnar, 2004) and *in situ* stresses resulting from the tectonic and erosional history of the bedrock (Amadei and Stephansson, 1997). Leith et al. (2010, 2011) suggested that differential stresses in inherently highly-stressed bedrock are responsible for at least some of the extensive fracture systems commonly observed in deglaciated terrains. According to this view, *in situ* rock stresses provide the maximum principal stress to near-surface bedrock, and the development of pronounced differential stresses during deglaciation reflects reduction in confining stress as ice loading is reduced during deglaciation. For tectonically stable terrains, McColl (2012) conceptualized the issue in terms of high surface-parallel stresses induced in two possible ways: (1) release of stress perpendicular to the slope by glacial erosion and/or glacial unloading, whilst slope-parallel confining stresses are maintained by the surrounding rock mass; and (2) increase in topographic stress concentration due to self-weight loading when confining stresses are removed by glacial erosion and/or unloading by ice.

Irrespective of the cause of deglacial stress release, it is widely accepted that it is responsible for fracture propagation within deglacially-unloaded rock slopes, and in particular for the development of slope-parallel sheeting joints (Hencher et al., 2011; McColl, 2012) that form potential failure planes. Such joints are widespread on crystalline rocks in our study areas (Glasser, 1997) and planar or stepped failure surfaces at some RSF sites demonstrate their importance in RSF release (e.g. Ballantyne and Stone, 2004; Ballantyne, 2013). Some researchers, however, have rejected deglacial stress release as a cause of RSFs where a millennial-scale delay separates the timing of deglaciation from that of failure (Mitchell et al., 2007; Dortch et al., 2009; Hippolyte et al., 2009; Prager et al., 2009; Stock and Uhrhammer, 2010). This interpretation is convincingly challenged by Eberhardt et al. (2004) and Gugliemi and Cappa (2010), who demonstrated that stress changes accompanying Late Pleistocene deglaciation may initiate time-dependent rock mass strength degradation over millennial timescales through progressive shear plane development within fractured rock masses (cf. Kemeny, 2003; Prager et al., 2008; Brideau et al., 2009). This view is supported by the work of Cossart et al. (2008), who showed that, irrespective of timing, RSFs in the western Alps are located in areas where reduction of glacially-induced confining stresses was greatest.

An implication of this interpretation is that stress release initiated by Late Pleistocene deglacial unloading may result in spontaneous kinematic release of rock long after deglaciation, without involvement of any extrinsic trigger mechanism. Thus the pattern of timing of postglacial RSFs in Fig. 4a and d may simply reflect the duration of progressive rock-mass weakening to the point of catastrophic failure, with ~90% of dated RSFs occurring within 5000 years after deglaciation and the remainder over the following five millennia. An alternative interpretation is that although stress-release may have preconditioned failure through time-dependent rock mass weakening, the timing of failure, at least in some cases, represents extrinsic triggering. Possible triggering mechanisms are considered below.

8.2. Debuttressing

The term 'debuttressing' is used the describe the removal of supporting glacier ice from potentially unstable rockwalls, and has been cited by several authors as a cause of failure during or immediately after Late Pleistocene deglaciation (e.g. Agliardi et al., 2009; Ivy-Ochs et al., 2009; Hippolyte et al., 2012). Both large-scale rock-slope deformation and catastrophic failure of rock slopes has occurred during recent downwastage of valley glaciers (e.g. Bovis, 1990; Sigurdsson and Williamson, 1991; McSaveney, 1993; Evans and Clague, 1994; Holm et al., 2004) lending support to this view, though McColl and Davies (2013) have argued that because glacier ice is liable to deform under stresses imposed by an adjacent unstable rock mass, complete debuttressing is not a prerequisite for movement of ice-contact rock slopes.

Debuttressing implies that slope failure occurs during or immediately after deglaciation in response to the loss of support of glacier ice, and hence that RSF age should be statistically indistinguishable from deglaciation age. This is true for only nine (29%) of our 31 dated RSFs, including the two that failed on to YDS glaciers; all other are significantly younger ($p < 0.05$) than the inferred timing of deglaciation, demonstrating that debuttressing was not instrumental in triggering failure in the great majority of cases. Moreover, the large uncertainties associated with both inferred deglaciation ages and RSF ages (Table 1) mean that some of the nine 'rapid response' RSFs could have occurred several centuries after complete deglaciation of the RSF site. Debuttressing therefore appears to offer a possible explanation for only a small minority of the RSFs in our sample. It is also notable that of >500 postglacial RSFs documented in the Scottish Highlands (Ballantyne, 1986; Jarman, 2006), only three or four cases of RSF runout on to former glacier surfaces have been reported (Ballantyne, 2013), including sites 22 and 23, again suggesting that debuttressing has been of minor significance.

8.3. Palaeoseismicity

It has long been recognized that many major RSFs are triggered by earthquakes, particularly in tectonically active mountain belts (Keefer, 1984, 1994; Meunier et al., 2007), and numerous postglacial RSFs have been attributed to seismic activity (e.g. Hormes et al., 2008; Antinao and Gosse, 2009; Sanchez et al., 2010; Stock and Uhrhammer, 2010). Simulations by McColl et al. (2012) suggest that thick ice cover substantially reduces ground motion during earthquakes but that this mitigating effect diminishes markedly as ice downwastes during deglaciation. According to Eisbacher and Clague (1984), large rock avalanches are typically precipitated by seismic events of magnitude $M \geq 6.0$, though smaller RSFS may occur at lower magnitudes and much depends on the pre-seismic state of stress and fracture continuity within a rock mass. Moreover, even where earthquake intensities are insufficient to trigger immediate kinematic release, dynamic loading during earthquakes may accelerate fracture propagation, thus promoting subsequent rock-mass failure (Prager et al., 2008).

Our study area presently experiences relative tectonic stability. Recent seismic events with $M_L > 4.0$ are rare and focused near the western seaboard of Scotland (Musson, 2007). Several authors, however, have proposed that tectonically-stable intraplate terrains, including the Scottish Highlands, experienced high-magnitude earthquake activity during and after shrinkage of Late Pleistocene glaciers (Sissons and Cornish, 1982; Dehls et al., 2000; Morner, 2004, 2005; Lagerbäck and Sundh, 2008; Strasser et al., 2013). Such enhanced seismicity has been attributed to fault (re)activation due to differential glacio-isostatic crustal rebound acting in conjunction with elastically stored tectonic stresses, though

because of the prolonged response time of the resulting changes in crustal stress, fault activation and associated seismic activity may lag deglaciation by centuries or millennia (Muir-Wood, 2000; Stewart et al., 2000). There is evidence in northern Ireland for metre-scale normal faulting triggered by ice unloading during the final stages of glaciation (Knight, 1999). In the Scottish Highlands, postglacial crustal rebound and associated faulting produced metre-high scarps (Firth and Stewart, 2000; Stewart et al., 2001), and soft-sediment deformation structures of Lateglacial or early Holocene age have been interpreted as the products of $M \approx 4.6$–6.4 earthquakes (Davenport and Ringrose, 1987; Ringrose, 1989a, 1989b; Stewart et al., 2001). The available evidence is therefore consistent with enhanced seismicity during the Lateglacial period, though the magnitude and timing of such activity is poorly constrained (Firth and Stewart, 2000).

If earthquakes played a major role in triggering postglacial RSFs in Scotland and NW Ireland, a correspondence between RSF ages and the timing of rapid crustal rebound is to be expected. The available data on crustal rebound rates are limited, but suggest that at least a broad correspondence exists (Fig. 5). For a site at Arisaig on the west coast of Scotland (Fig. 1), for example, maximum rates of crustal uplift (14.3–26.7 mm a^{-1}) occurred during the period ~15.7–12.7 ka (Firth and Stewart, 2000), coinciding with the timing of all dated RSFs on Jura (10–14), 110 km to the south. After ~12.7 ka average rates of uplift diminished markedly, as does the frequency of dated RSFs (Fig. 5), suggesting that the two may be linked through seismic triggering of RSFs by uplift-driven earthquake activity. This link may also explain the abrupt change in the frequency of dated RSFs at ~11.7 ka (Fig. 3): prior to ~12.7 ka, average rates of rebound at all sites for which data are available averaged 14.3–31.5 mm a^{-1}; after ~10.7 ka, average uplift rates at all sites fall below 7.3 mm a^{-1} (Firth and Stewart, 2000).

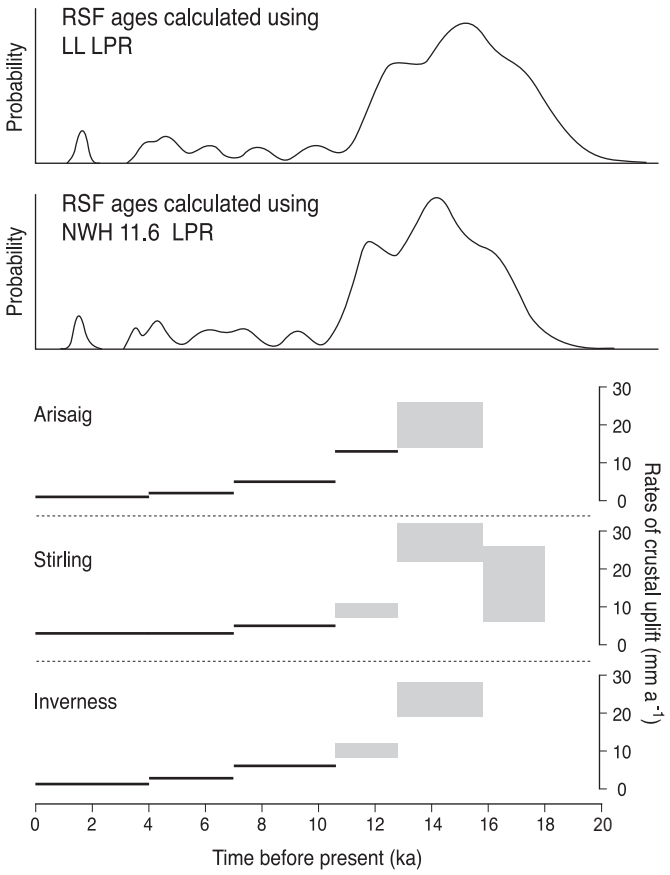

Fig. 5. Probability density distributions for all RSF ages ($n = 31$) plotted against average rates of glacio-isostatic crustal uplift for three locations in Scotland (Fig. 1). Crustal uplift data are from Firth and Stewart (2000).

Low-resolution temporal coincidence between uplift rates and RSF frequency (Fig. 5) is not proof of seismic causation, but the morphology of most dated RSFs is also consistent with seismic triggering. In every case where there is a clear failure plane it extends to, or near to, the crest of the slope (Fig. 2). Densmore and Hovius (2000) have shown that such full-slope failures are characteristic of coseismic RSFs, as topographic amplification of ground acceleration during earthquakes tends to trigger failure at or near ridge crests (Geli et al., 1988; Murphy, 2006). Both temporal association and failure plane morphology therefore suggest that the role of uplift-driven seismicity in triggering failure of fractured bedrock has been much more important in glaciated mountains of the British Isles than some studies suggest (e.g. Jarman, 2006).

An additional possible explanation of the temporal association between Lateglacial RSFs and rapid isostatic uplift is that the latter may have been responsible for large-scale lateral dilation (spreading) of mountain rock masses. Cossart et al. (2013b) have suggested that such dilation can generate slope-parallel fractures, normal (extensional) faulting and deep-seated gravitational slope deformation. Examples of gravitational rock-slope deformations are common on mountains in the British Isles, particularly on metasedimentary rocks (Jarman, 2006, 2007), and some of the dated RSFs in this study may represent catastrophic failure of slopes weakened by progressive deformation. The possible role of uplift-induced lateral dilation of mountain ridges in causing fracture propagation and pre-failure creep cannot, however, be assessed without greater understanding of the age, structure and evolution of extant 'unfailed' gravitational slope deformations, informed by theoretical assessment of the magnitude of dilation and dilation-induced stresses likely to be induced by non-uniform isostatic rebound.

8.4. Climatically-induced triggers

Three climatically-driven factors have been suggested by McColl (2012) as possible triggers of paraglacial RSFs: high joint water pressures, frost wedging and permafrost degradation. The millennial-scale delay between deglaciation and failure at over 70% of our RSFs implies that high joint-water pressures associated with deglaciation played no part in triggering failure at these sites. We cannot exclude the possibility that failure was in some cases triggered by build-up of joint-water pressures during exceptional rainstorms, but as Densmore and Hovius (2000) have shown, rainstorm-triggered RSFs tend to occur on lower slopes, and in all or nearly all cases our sampled RSFs extend to the slope crest. Frost wedging due to recurrent (seasonal) freezing of water and thawing of ice in joint appears unlikely to trigger deep-seated RSFs, as even under propitious conditions annual freeze-thaw cycles affect at most the outermost few metres of rock slopes (Matsuoka, 1994; Matsuoka et al., 1998), and near-saturation of the joint network is required for frost wedging to be effective. It is notable, too that the timing of dated RSFs (Table 1; Figs. 3 and 6) spans both stadial conditions (prior to ~14.7 ka and during the YDS of ~12.9–11.7 ka), when annual freeze thaw cycles must have been limited to the former active layer, and cool temperate conditions (during the Lateglacial Interstade of ~14.7–12.9 ka and the Holocene) when annual freeze-thaw depths were limited by depth of winter freezing. Thermistor measurements made of depth of freezing within joints on a sandstone cliff at 600 m altitude in NW Scotland (Ballantyne, unpublished data) suggest that present frost penetration is limited to the outermost 0.6–1.1 m of the joint network.

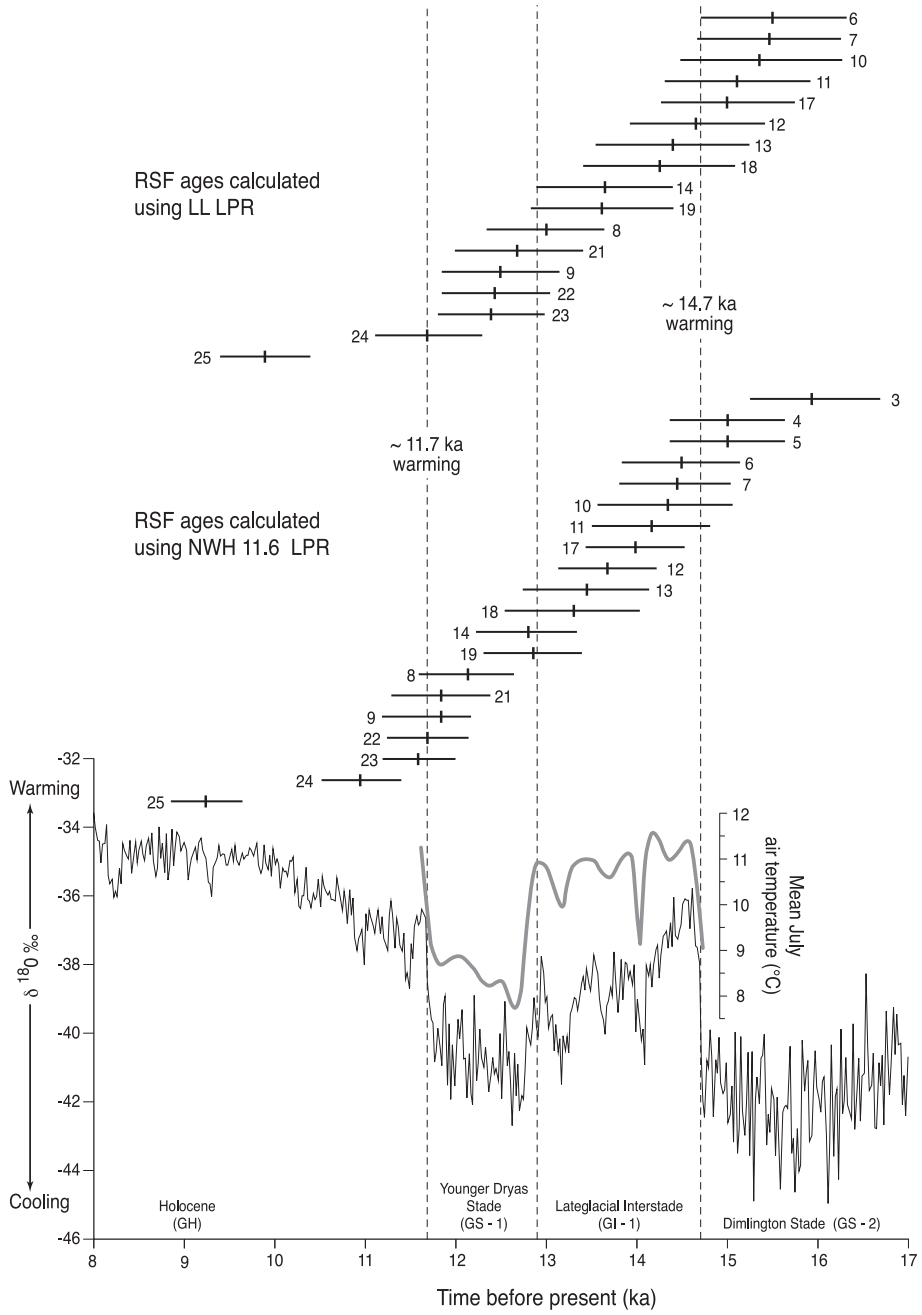

Fig. 6. Weighted mean ages (vertical dashes) and external ± 1σ uncertainties (horizontal bars) plotted against NGRIP ice core $\delta^{18}O$ data for 17–8 ka (Rasmussen et al., 2006), the ice core stages proposed by Lowe et al. (2008) and mean annual temperature data inferred from chironomid assemblages in SE Scotland (Brooks and Birks, 2000) matched to the NGRIP ice core data. RSFS older than 16.0 ka or younger than 8.0 ka are not shown.

Permafrost degradation leading to warming and thaw of ice-bonded rock represents an important cause of rock-mass weakening and failure in areas of alpine permafrost under warming temperatures (e.g. Davies et al., 2001; Fischer et al., 2006; Gruber and Haeberli, 2007; Allen et al., 2010; Krautblatter et al., 2012, 2013). Permafrost is known to have developed in the British Isles both in the aftermath of ice-sheet deglaciation and during the YDS (Ballantyne and Harris, 1994), so it is possible that permafrost degradation triggered RSFs during periods of climatic warming. During the postglacial period there have been two periods of very rapid warming that terminated stadial conditions: at the Dimlington Stade-Lateglacial Interstade transition at ~14.7 ka, and the YDS-Holocene transition at ~11.7 ka (Brooks and Birks, 2000; Brooks et al., 2012). Nine RSF ages (LL LPR) or 11 RSF ages (NWH11.6 LPR) overlap with one or other of these periods of rapid warming at ± 1σ (Fig. 6), though only four RSF ages (LL LPR) or six RSF ages (NWH11.6 LPR) either coincide with or occur within 500 years after these warming periods. We therefore cannot exclude the possibility that warming and thaw of permafrost ice in joints triggered kinematic release in a few cases, but the timing of the great majority of dated RSFS appears to be independent of periods of rapid warming.

9. Discussion

Several interesting features emerge from the temporal patterns of RSF response to deglaciation summarised in Fig. 4. Although

almost all sampled RSFs at sites deglaciated by ice-sheet retreat occurred within 5000 years following deglaciation (Fig. 4b and e), RSF activity did not peak immediately following deglaciation as suggested by Cruden and Hu (1993), Soldati et al. (2004) and others, but roughly 1000–3000 years after ice-sheet deglaciation. As argued above, this long delay probably reflects progressive rock-mass weakening initiated by deglacial stress release and associated tensile rock mass damage. According to Eberhardt et al. (2004) and Gugliemi and Cappa (2010), deglaciated rock masses may experience millennial-scale stability without major changes in kinematic state. During this pre-failure period, redistributed stress concentrations intensify fracture propagation and coalescence within surface-parallel damage zones, leading to progressive loss of stability through shearing of intact rock bridges and possible ductile deformation until catastrophic failure occurs, either spontaneously or in response to an extrinsic trigger. The broad temporal coincidence between maximum rates of glacio-isostatic uplift and maximum RSF activity (Fig. 5) suggests that seismic activity may have been important in triggering failure of some fractured rock masses, particularly prior to ~12 ka.

The difference in timing of response between sites deglaciated by ice sheet retreat (Fig. 4b and e) and those deglaciated during retreat of YDS glaciers (Fig. 4c and f) may also, as suggested above, reflect reduced seismic activity during the Holocene due to diminishing rates of crustal uplift. An alternative explanation lies in contrasts in the duration and dimensions of ice-sheet glaciation and those of glaciation during the YDS. An extensive ice sheet was present over the northern parts of the British Isles for roughly 15,000 years from ~30 ka to ~15 ka (Bradwell et al., 2008; Ballantyne, 2010; Clark et al., 2012) during which time its volume and configuration fluctuated markedly (Hubbard et al., 2009). For much of this period, ice extended far out on to adjacent shelves and ice buried all summits in NW Ireland and Scotland, implying ice thicknesses at least 1000 m above valley floors, and probably much more, in the Scottish Highlands (Fabel et al., 2012). Conversely, most YDS glaciers in the Scottish Highlands existed for less than ~1200 years, were confined to glacial troughs at the sites of sampled RSFs and accomplished very limited modification of the pre-YDS landscape (Golledge, 2007; Golledge et al., 2008; Golledge, 2010). The absence of a pronounced peak in RSF activity following YDS deglaciation may therefore reflect comparatively limited (and comparatively brief) glacial re-loading and unloading of rock slopes at this time. Jarman (2006) has suggested that even though most RSFs in the Scottish Highlands occur within YDS glacier limits, failure at such sites primarily reflected 'slope stresses' engendered by ice-sheet loading and unloading rather than the effects of glacial reoccupation during the YDS. The absence of a post-deglaciation peak in RSF activity in Fig. 4c and f is consistent with this view. We note, however, that we cannot exclude the possibility that the contrast in response represents differences in lithology (Sellier, 2008). The post-deglaciation peak in RSF activity evident in Fig. 4b and e was generated by dates obtained on quartzite, granite and sandstone RSFs (Table 1), whereas most dated RSFs inside the YDS glacier limits are seated on schist. It is possible that the pre-release lag in response to deglaciation differs systematically amongst lithologies.

An implication of the temporal pattern of RSFs at sites not reoccupied by glacier ice during the YDS (Fig. 4b and e) is that numerous RSFs must also have occurred inside the limits of YDS glaciation in valleys that were completely deglaciated during the Lateglacial Interstade (~14.7–12.9 ka), but these have not been recorded in RSF inventories (Ballantyne, 1986; Jarman, 2006) because YDS glacier ice subsequently removed RSF runout debris. Such RSF sites can be identified by 'empty' failure scars comprising a steep headwall and subjacent planar or stepped failure surface. Although no systematic survey of such sites has been carried out, it is possible that Lateglacial RSFs that occurred before or during YDS glaciation made a substantial contribution to the sediment load of YDS glaciers in Scotland and elsewhere (Ballantyne, 2002, 2013).

More generally, our results support the results of previous research in Scandinavia (Morner, 2004; Blikra et al., 2006; Longva et al., 2009) and central Switzerland (Prager et al., 2008) indicating that the shrinkage of Late Pleistocene ice sheets on tectonically-stable intraplate steepland terrains was followed by a period of greatly enhanced RSF activity extending over a few millennia. It seems likely that deglacial stress release and progressive pre-failure rock mass weakening through fracture propagation, rock-mass deformation and possibly large-scale uplift-induced mountain dilation played a key role in preconditioning and triggering failure, though seismic activity driven by rapid rates of glacio-isostatic recovery may have precipitated kinematic release of fractured rock masses, particularly during the Lateglacial period of maximum uplift rates. Glacial debuttressing, thaw of ice-bonded rock, frost wedging and high joint-water pressures are inferred to have been of less importance in triggering postglacial RSFs in such areas.

10. Conclusions

1. A sample of 31 RSFs in Scotland and NW Ireland dated using cosmogenic ^{10}Be or ^{36}Cl span almost the full period following retreat of the last British-Irish Ice Sheet, from 18.2 ± 1.2 ka to 1.7 ± 0.2 ka or 17.1 ± 1.0 ka to 1.5 ± 0.1 ka, depending on the production rate used in ^{10}Be age calibration. Our sample indicates that rock slope failure was roughly 4.6 times more frequent during the Lateglacial period (>11.7 ka) than during the Holocene, but there is no evidence for significant clustering within either period.
2. 95% of dated RSFs at sites deglaciated during the shrinkage of the last ice sheet occurred within ~5400 years following deglaciation, with a peak of RSF activity 1600–1700 years after deglaciation. By contrast, RSFs deglaciated by retreat of valley glaciers at the end of the YDS (~12.9–11.7 ka) show no clear temporal pattern, with RSF ages scattered throughout the Holocene.
3. We infer that stress release and resulting fracture propagation due to deglacial unloading, and particularly the development of sheeting joints under tensile stress conditions, was the key factor in preconditioning or triggering kinematic release of rock masses following ice-sheet deglaciation. The millennial-scale time lag between ice-sheet deglaciation and peak RSF activity is inferred to represent time-dependent rock mass strength degradation through progressive failure plane development within fractured rock masses, leading to either spontaneous catastrophic failure or failure triggered by an extrinsic agent. Tensile stresses induced by uplift-driven dilation of mountain masses may have abetted pre-failure rock-mass weakening.
4. The timing of failure following deglaciation suggests that only a minority of failures (<29%) could have been triggered by debuttressing due to glacier downwastage; the ages of all others significantly postdate the timing of deglaciation, typically by >1000 years. For similar reasons enhanced joint-water pressures during deglaciation can only have influenced a small proportion of failures. Frost wedging is unlikely to have acted as a failure trigger as annual freeze-thaw cycles were probably too shallow to initiate deep-seated failure. Because the timing of only 4–6 dated RSFs coincides with, or postdates by <500 years, periods of rapid (stadial to interstadial) warming at ~14.7 ka and ~11.7 ka, we infer that warming and thaw of permafrost ice in joints may have triggered failure in only a few cases; all other

RSFs apparently occurred under full-stadial conditions or >500 years after stadial to interstadial warming.

5. Conversely, the timing of maximum RSF activity broadly coincides with the timing of maximum rates of glacio-isostatic crustal rebound in Scotland, suggesting a causal connection via fault (re)activation and triggering of failure by earthquakes, especially during the Lateglacial period. This interpretation is consistent with failure extending to ridge or plateau crests in all cases where the failure plane is well defined, and may explain the diminished frequency of RSFS during the Holocene, when uplift rates were much slower.
6. The absence of a significant peak of RSF activity following deglaciation at the end of the YDS implies that YDS glacial erosion and re-loading/unloading of rock masses by valley glaciers during the stadial was relatively ineffective in preconditioning a further cycle of enhanced RSF activity, though we cannot exclude the possibility that the observed contrast between post-ice sheet and post-YDS deglacial RSF response may in part reflect differing lithologies in the two subsamples.
7. Numerous RSFs must have occurred inside the limits of YDS glaciation prior to and during the readvance of glacier ice at this time. Such RSFs are represented by failure scars lacking runout debris, and suggest that reworked RSF runout debris may have contributed substantially to the sediment budget of YDS glaciers.

Our sample of RSF ages confirms that retreat of Late Pleistocene ice sheets in tectonically-stable, mountainous intraplate terrains initiated a period of enhanced rock-slope failure over a period of roughly 5000 years spanning the Lateglacial period and very early Holocene. It follows that the great majority of undated RSFs in such areas are also of Lateglacial or early Holocene age. Equally, however, the late Holocene ages of a few dated RSFs imply that future catastrophic RSFs are possible, especially in areas occupied by glacier ice during the YDS. Future research priorities include dating of postglacial fault scarps to investigate more directly the temporal connection between palaeoseismicity and Lateglacial RSFs (cf. Sanchez et al., 2010), and establishing the ages of deep-seated gravitational deformations, which constitute many of the largest RSFs in the British Isles but have not hitherto been dated.

Acknowledgements

We are grateful to the Carnegie Trust for the Universities of Scotland and the UK Natural Environment Research Council Cosmogenic Isotope Facility (NERC-CIAF project 9046-0308) for funding the dating programme, and the Carnegie Trust and British Society for Geomorphology for supporting fieldwork in Scotland. We acknowledge in particular the debt we owe to Bob Finkel, Delia Gheorghiu, Joy Laydbak, Angel Rodés, Dylan Rood, Christoph Schnabel and Sheng Xu for sample preparation or AMS analysis. We also thank Derek Fabel for permission to use the LL LPR calibration dataset in advance of publication, David Jarman, Bernie Lafferty, Sam Smyth, and Dave Southall for assistance in sample collection, and Aaron Putnam and two anonymous reviewers for constructive comments on the original manuscript. David Jarman is also thanked for suggesting suitable sampling sites during the early stages of this research.

References

Abele, G., 1997. The influence of glacier and climatic variations on rockslide activity in the Alps. Paläoklimaforschung 19, 1–6.
Agliardi, F., Crosta, G.B., Zanchi, A., Ravazzi, C., 2009. Onset and timing of deep-seated gravitational slope deformations in the eastern Alps, Italy. Geomorphology 103, 113–129.
Allen, S., Cox, S., Owens, I., 2010. Rock avalanches and other landslides in the central Southern Alps of New Zealand: a regional study considering possible climate change impacts. Landslides 8, 33–48.
Amadei, B., Stephansson, O., 1997. Rock Stress and its Measurement. Chapman and Hall, London.
Antinao, J.L., Gosse, J., 2009. Large rockslides in the southern central Andes of Chile (32–34.5°S): tectonic control and significance for Quaternary landscape evolution. Geomorphology 104, 117–133.
Arsenault, A.M., Meigs, A.J., 2005. Contribution of deep-seated bedrock landslides to erosion of a glaciated basin in southern Alaska. Earth Surf. Process. Landf. 30, 1111–1125.
Augustinus, P.C., 1995. Glacial valley cross-profile development: the influence of in situ rock stress and rock mass strength, with examples from the Southern Alps, New Zealand. Geomorphology 14, 87–97.
Balco, G., 2011. Contributions and unrealized potential contributions of cosmogenic-nuclide exposure dating to glacier chronology, 1990–2010. Quat. Sci. Rev. 30, 3–27.
Balco, G., Briner, J., Finkel, R.C., Rayburn, J.A., Ridge, J.C., Schaefer, J.M., 2009. Regional beryllium-10 production rate calibration for late-glacial northeastern North America. Quat. Geochronol. 4, 93–107.
Balco, G., Stone, J.O., Lifton, N.A., Dunai, T.J., 2008. A complete and easily accessible means of calculating surface exposure ages or erosion rates from ^{10}Be and ^{26}Al measurements. Quat. Geochronol. 3, 174–195.
Ballantyne, C.K., 1986. Landslides and slope failures in Scotland: a review. Scott. Geogr. Mag. 102, 134–150.
Ballantyne, C.K., 2002. Paraglacial geomorphology. Quat. Sci. Rev. 21, 1935–2017.
Ballantyne, C.K., 2010. Extent and deglacial chronology of the last British–Irish ice sheet: implications of exposure dating using cosmogenic isotopes. J. Quat. Sci. 25, 515–534.
Ballantyne, C.K., 2012. Chronology of glaciation and deglaciation during the Loch Lomond (Younger Dryas) Stade in the Scottish Highlands: implications of recalibrated ^{10}Be exposure ages. Boreas 41, 513–526.
Ballantyne, C.K., 2013. Lateglacial rock-slope failures in the Scottish Highlands. Scott. Geogr. J. 129, 67–84.
Ballantyne, C.K., Harris, C., 1994. The Periglaciation of Great Britain. Cambridge University Press, Cambridge.
Ballantyne, C.K., Stone, J.O., 2004. The Beinn Alligin rock avalanche, NW Scotland: cosmogenic ^{10}Be dating, interpretation and significance. Holocene 14, 448–453.
Ballantyne, C.K., Stone, J.O., 2009. Rock-slope failure at Baosbheinn, Wester Ross, NW Scotland: age and interpretation. Scott. J. Geol. 45, 177–181.
Ballantyne, C.K., Stone, J.O., 2012. Did large ice caps persist on low ground in northwest Scotland during the Lateglacial Interstade? J. Quat. Sci. 27, 297–306.
Ballantyne, C.K., Stone, J.O., 2013. Timing and periodicity of paraglacial rock-slope failures in the Scottish Highlands. Geomorphology 186, 150–161.
Ballantyne, C.K., McCarroll, D., Stone, J.O., 2007. The Donegal ice dome, northwest Ireland: dimensions and chronology. J. Quat. Sci. 22, 773–783.
Ballantyne, C.K., Schnabel, C., Xu, S., 2009a. Exposure dating and reinterpretation of coarse debris accumulations ('rock glaciers') in the Cairngorm Mountains, Scotland. J. Quat. Sci. 24, 19–31.
Ballantyne, C.K., Schnabel, C., Xu, S., 2009b. Readvance of the last British-Irish ice sheet during Greenland Interstade 1 (GI-1): the Wester Ross Readvance, NW Scotland. Quat. Sci. Rev. 28, 783–789.
Ballantyne, C.K., Stone, J.O., Fifield, L.K., 1998. Cosmogenic Cl-36 dating of postglacial landsliding at The Storr, Isle of Skye, Scotland. Holocene 8, 347–351.
Ballantyne, C.K., Wilson, P., Gheorghiu, D., Rodés, A., 2013a. Enhanced rock-slope failure following ice-sheet deglaciation: timing and causes. Earth Surf. Process. Landf.. http://dx.doi.org/10.1002/esp.3495.
Ballantyne, C.K., Wilson, P., Schnabel, C., Xu, S., 2013b. Lateglacial rock-slope failures in NW Ireland: age, causes and implications. J. Quat. Sci.. http://dx.doi.org/10.1002/jqs.2675.
Bigot-Cormier, F., Braucher, R., Bourlès, D., Guglielmi, Y., Dubar, M., Stéphan, J.-F., 2005. Chronological constraints on processes leading to large landslides. Earth Planet. Sci. Lett. 235, 141–150.
Blikra, L.H., Longva, O., Braathen, A., Dehls, J.F., Stalsberg, K., 2006. Rock slope failures in Norwegian Fjord areas: examples, spatial distribution and temporal pattern. In: Evans, S.G., Mugnozza, G.S., Strom, A., Hermanns, R.L. (Eds.), Landslides from Massive Rock Slope Failure. Springer, Dordrecht, pp. 475–496.
Bovis, M.J., 1990. Rock-slope deformation at Affliction Creek, southern coast mountains, British Columbia. Can. J. Earth Sci. 27, 243–254.
Braathen, A., Blikra, L.H., Berg, S.S., Karlsen, F., 2004. Rock-slope failures in Norway; type, geometry, deformation mechanisms and stability. Nor. J. Geol. 84, 67–88.
Bradwell, T., Stoker, M.S., Golledge, N.R., Wilson, C.K., Merritt, J.W., Long, D., Everest, J.D., Hestvik, O.B., Stevenson, A.G., Hubbard, A.L., Finlayson, A.G., Mathers, H.E., 2008. The northern sector of the last British Ice Sheet: maximum extent and demise. Earth Sci. Rev. 88, 207–226.
Brideau, M.-A., Yan, M., Stead, D., 2009. The role of tectonic damage and brittle rock failure in the development of large rock failures. Geomorphology 103, 30–49.
Brooks, S.J., Birks, H.J.B., 2000. Chironomid-inferred Late-glacial air temperatures at Whitrig Bog, southeast Scotland. J. Quat. Sci. 15, 759–764.
Brooks, S.J., Matthews, I.P., Birks, H.H., Birks, H.J.B., 2012. High resolution Lateglacial and early-Holocene summer air temperature records from Scotland inferred from chironomid assemblages. Quat. Sci. Rev. 41, 67–82.
Clark, C.D., Hughes, A.L.C., Greenwood, S.L., Jordan, C., Sejrup, H.P., 2012. Pattern and timing of retreat of the last British–Irish Ice Sheet. Quat. Sci. Rev. 44, 112–146.

Clark, J., McCabe, A.M., Schnabel, C., Clark, P.U., Freeman, S., Maden, C., Xu, S., 2009. ^{10}Be chronology of the last deglaciation of County Donegal, northwestern Ireland. Boreas 38, 111–118.
Cossart, É., Braucher, R., Fort, M., Bourlès, D.L., Carcaillet, J., 2008. Slope instability in relation to glacial debuttressing in alpine areas (Upper Durance catchment, southeastern France): evidence from field data and ^{10}Be cosmic ray exposure ages. Geomorphology 95, 3–26.
Cossart, É., Mercier, D., Decaulne, A., Feuillet, T., 2013a. An overview of the consequences of paraglacial landsliding on deglaciated mountain slopes: typology, timing and contribution to cascading fluxes. Quaternaire 24, 13–24.
Cossart, É., Mercier, D., Decaulne, A., Feuillet, T., Jónsson, H.P., Sæmundsson, Þ., 2013b. Impacts of post-glacial rebound on landslide spatial distribution at a regional scale in Northern Iceland (Skagafjörður). Earth Surf. Process. Landf.. http://dx.doi.org/10.1002/esp.3450.
Crosta, G.B., Frattini, P., Agliardi, F., 2013. Deep seated gravitational slope deformations in the European Alps. Tectonophysics 605, 13–33.
Cruden, D., Hu, X.Q., 1993. Exhaustion and steady state models for predicting landslide hazards in the Canadian Rocky Mountains. Geomorphology 8, 279–285.
Davenport, C.A., Ringrose, P.S., 1987. Deformation of Scottish Quaternary sediment sequences by strong earthquake motions. Geol. Soc. Spec. Publ. 29, 299–314.
Davenport, C.A., Ringrose, P.S., Becker, A., Hancock, P., Fenton, C., 1989. Geological investigations of Late- and Postglacial earthquake activity in Scotland. In: Gregersen, S., Basham, P. (Eds.), Earthquakes at North Atlantic Passive Margins: Neotectonics and Postglacial Rebound. Kluwer, Dordrecht, pp. 175–194.
Davies, M.C.R., Hamza, O., Harris, C., 2001. The effect of rise in mean annual temperature on the stability of rock slopes containing ice-filled discontinuities. Permafr. Periglac. Process. 12, 137–144.
Dehls, J.F., Olesen, O., Olsen, L., Blikra, L.H., 2000. Neotectonic faulting in northern Norway; the Stuoragurra and Nordmannvikdalen postglacial faults. Quat. Sci. Rev. 19, 1447–1460.
Densmore, A.L., Hovius, N., 2000. Topographic fingerprints of bedrock landslides. Geology 28, 371–374.
Dortch, J.M., Owen, L.A., Haneberg, W.C., Caffee, M.W., Dietsch, C., Kamp, U., 2009. Nature and timing of large landslides in the Himalaya and Transhimalaya of northern India. Quat. Sci. Rev. 28, 1037–1054.
Eberhardt, E., Stead, D., Coggan, J.S., 2004. Numerical analysis of initiation and progressive failure in natural rock slopes – the 1991 Randa rockslide. Int. J. Rock Mech. Min. Sci. 41, 69–87.
Eisbacher, G.H., Clague, J.J., 1984. Destructive Mass Movements in High Mountains: Hazard and Management. Geological Survey of Canada. Paper 84/16, 1–230.
El Bedoui, S., Gugliemi, Y., Lebourg, T., Pérez, J.-L., 2009. Deep-seated failure propagation in a fractured rock slope over 10,000 years: the La Clapière slope, the south-eastern French Alps. Geomorphology 105, 232–238.
Evans, S.G., Clague, J.J., 1994. Recent climate change and catastrophic geomorphic processes in mountain environments. Geomorphology 10, 107–128.
Everest, J.D., Kubik, P.W., 2006. The deglaciation of eastern Scotland: cosmogenic ^{10}Be evidence for a Lateglacial stillstand. J. Quat. Sci. 21, 95–104.
Fabel, D., Ballantyne, C.K., Xu, S., 2012. Trimlines, blockfields, mountain-top erratics and the vertical dimensions of the last British–Irish Ice Sheet in NW Scotland. Quat. Sci. Rev. 55, 91–102.
Fauqué, L., Hermanns, R.L., Hewitt, K., Rosas, M., Wilson, C., Baumann, V., Lagorio, S., Di Tommaso, I., 2009. Mega-deslizamientos de la pared sur del Cerro Aconcagua y su relación con depósitos asignados a la glaciación Pleistocena. Rev. la Asoc. Geol. Argent. 65, 691–712.
Finlayson, A., Golledge, N.R., Bradwell, T., Fabel, D., 2011. Evolution of a Lateglacial mountain icecap in northern Scotland. Boreas 40, 536–554.
Firth, C.R., Stewart, I.S., 2000. Postglacial tectonics of the Scottish glacio-isostatic uplift centre. Quat. Sci. Rev. 19, 1469–1493.
Fischer, L., Kääb, A., Huggel, C., Noetzli, J., 2006. Geology, glacier retreat and permafrost degradation as controlling factors of slope stability in a high mountain rockwall. Nat. Hazards Earth Syst. Sci. 6, 761–772.
Geli, L., Bard, P.-Y., Jullien, B., 1988. The effect of topography on earthquake ground motion: a review and new results. Seismol. Soc. Am. Bull. 78, 42–63.
Glasser, N.F., 1997. The origin and significance of sheet joints in the Cairngorm granite. Scott. J. Geol. 33, 125–131.
Golledge, N.R., 2007. Sedimentology, stratigraphy and glacier dynamics, western Scottish Highlands. Quat. Res. 68, 79–95.
Golledge, N.R., 2010. Glaciation of Scotland during the Younger Dryas Stadial: a review. J. Quat. Sci. 25, 550–566.
Golledge, N.R., Hubbard, A., Sugden, D.E., 2008. High-resolution numerical simulation of Younger Dryas glaciation in Scotland. Quat. Sci. Rev. 27, 888–904.
Gregerson, S., Basham, P.W. (Eds.), 1989. Earthquakes at North Atlantic Passive Margins: Neotectonics and Postglacial Rebound. Kluwer, Dordrecht.
Gruber, S., Haeberli, W., 2007. Permafrost in steep bedrock slopes and its temperature-related destabilization following climate change. J. Geophys. Res. 112, F02S18.
Gugliemi, Y., Cappa, F., 2010. Regional-scale relief evolution and large landslides: insights from geomechanical analyses in the Tinée Valley (southern French Alps). Geomorphology 117, 121–129.
Hencher, S.R., Lee, S.G., Carter, T.G., Richards, L.R., 2011. Sheeting joints: characterisation, shear strength and engineering. Rock Mech. Rock Eng. 44, 1–22.
Hermanns, R.L., Niedermann, S., 2011. Late Pleistocene–early Holocene palaeoseismicity deduced from lake sediment deformation and coeval landsliding in the Calchaquíes Valleys, NW Argentina. In: Geological Society of America Special Paper 479, pp. 181–194.
Hermanns, R.L., Niedermann, S., Ivy-Ochs, S., Kubik, P.W., 2004. Rock avalanching into a landslide-dammed lake causing multiple dam failure in Las Conchas valley (NW Argentina) – evidence from surface exposure dating and stratigraphic analyses. Landslides 1, 113–122.
Hermanns, R.L., Niedermann, S., Villanueva Garcia, A., Sosa Gomez, J., Strecker, M.R., 2001. Neotectonics and catastrophic failure of mountain fronts in the southern intra-Andean Puna Plateau, Argentina. Geology 29, 619–623.
Hewitt, K., Clague, J.J., Orwin, J.F., 2008. Legacies of catastrophic rock slope failures in mountain landscapes. Earth-Sci. Rev. 87, 1–38.
Hewitt, K., Gosse, J., Clague, J.J., 2011. Rock avalanches and the pace of Late Quaternary development of river valleys in the Karakoram Himalaya. Geol. Soc. Am. Bull. 123, 1836–1850.
Hippolyte, J.-C., Bourlès, D., Braucher, R., Carcaillet, J., Léanni, L., Arnold, M., Aumaître, G., 2009. Cosmogenic ^{10}Be dating of a sackung and its faulted rock glaciers, in the Alps of Savoy (France). Geomorphology 108, 312–320.
Hippolyte, J.-C., Bourlès, D., Léanni, L., Braucher, R., Chauvet, F., Lebatard, A.E., 2012. ^{10}Be ages reveal >12 ka of gravitational movement in a major sackung of the western Alps (France). Geomorphology 171–172, 139–153.
Holm, K., Bovis, M., Jakob, M., 2004. The landslide response of alpine basins to post-Little Ice Age glacial thinning and retreat in southwestern British Columbia. Geomorphology 57, 201–216.
Hormes, A., Ivy-Ochs, S., Kubik, P.W., Ferreli, L., Michetti, A.M., 2008. ^{10}Be exposure ages of a rock avalanche and a late glacial moraine in the Alta Valtellina, Italian Alps. Quat. Int. 190, 136–145.
Hubbard, A., Bradwell, T., Golledge, N.R., Hall, A.M., Patton, H., Sugden, D.E., Cooper, R., Stoker, M.S., 2009. Dynamic cycles, ice streams and their impact on the extent, chronology and deglaciation of the British–Irish Ice Sheet. Quat. Sci. Rev. 28, 758–776.
Ivy-Ochs, S., Poschinger, A.V., Synal, H.-A., Maisch, M., 2009. Surface exposure dating of the Flims landslide, Graubünden, Switzerland. Geomorphology 103, 104–112.
Jarman, D., 2006. Large rock-slope failures in the Highlands of Scotland: characterisation, causes and spatial distribution. Eng. Geol. 83, 161–182.
Jarman, D., 2007. Introduction to mass movements in the older mountain areas of Great Britain. In: Cooper, R.G. (Ed.), Mass Movements in Great Britain, Geological Conservation Review Series No 33. Joint Nature Conservation Committee, Peterborough, pp. 33–56.
Keefer, D.K., 1984. Landslides caused by earthquakes. Geol. Soc. Am. Bull. 95, 406–421.
Keefer, D.K., 1994. The importance of earthquake-induced landslides to long-term slope erosion and slope-failure hazards in seismically active regions. Geomorphology 10, 265–284.
Kellerer-Pirklbauer, A., Proske, H., Strasser, V., 2010. Paraglacial slope adjustment since the end of the Last Glacial Maximum and its long-lasting effects on secondary mass wasting processes: Hauser Kaibling, Austria. Geomorphology 120, 65–76.
Kemeny, J., 2003. The time-dependent reduction of sliding cohesion due to rock bridges along discontinuities: a fracture mechanics approach. Rock Mech. Rock Eng. 36, 27–38.
Knight, P., 1999. Geological evidence for neotectonic activity during deglaciation of the southern Sperrin Mountains, Northern Ireland. J. Quat. Sci. 14, 45–57.
Krautblatter, M., Funk, D., Günzel, F.K., 2013. Why permafrost rocks become unstable: a rock-ice-mechanical model in space and time. Earth Surf. Process. Landf. 38, 876–887.
Krautblatter, M., Huggel, C., Deline, P., Hasler, A., 2012. Research perspectives on unstable high-alpine bedrock permafrost: measurement, modelling and process understanding. Permafr. Periglac. Process. 23, 80–88.
Lagerbäck, R., Sundh, M., 2008. Early Holocene Faulting and Palaeoseismicity in Northern Sweden. Geological Survey of Sweden. Research Paper C836, 84 pp.
Lal, D., 1991. Cosmic ray labeling of erosion surfaces: in situ nuclide production rates and erosion models. Earth Planet. Sci. Lett. 104, 424–439.
Leith, K., Amann, F., Moore, J.R., Kos, A., Loew, S., 2010. Conceptual modelling of near-surface extensional fracture in the Matter and Saas Valleys, Switzerland. In: Williams, A.L., Pinches, G.M., Chin, C.Y., McMorran, T.J., Massey, C.I. (Eds.), Geologically Active: Proceedings of the 11th IAEG Congress, Auckland, New Zealand. CRC Press, Boca Raton, pp. 363–371.
Leith, K., Moore, J., Amann, F., Loew, S., 2011. Effect of Glacial Ice Cover on Fracturing Critically Stressed Bedrock. In: Geophysical Research Abstracts 13. EGU2011-12825-2.
Longva, O., Blikra, L.H., Dehls, J.F., 2009. Rock avalanches: distribution and frequencies in the inner part of Storfjorden, Møre og Romsdal County, Norway. Geological Survey of Norway, p. 32. Report 2009.002.
Lowe, J.J., Rasmussen, S.O., Björk, S., Hoek, W.J., Steffensen, J.P., Walker, M.J.C., Yu, Z.C., INTIMATE Group, 2008. Synchronisation of palaeoenvironmental events in the North Atlantic region during the Last Termination: a revised protocol recommended by the INTIMATE Group. Quat. Sci. Rev. 27, 6–17.
Macleod, A., Palmer, A.P., Lowe, J.J., Rose, J., Bryant, C., Merritt, J., 2011. Timing of glacier response to Younger Dryas climatic cooling in Scotland. Global Planet. Change 79, 264–274.
Matsuoka, N., 1994. Diurnal freeze-thaw depth in rockwalls: field measurements and theoretical considerations. Earth Surf. Process. Landf. 19, 423–455.
Matsuoka, N., Hirakawa, K., Watanabe, T., Haeberli, W., Keller, F., 1998. The role of diurnal, annual and millennial freeze-thaw cycles in controlling alpine slope

stability. In: Proceedings of the 7th International Conference on Permafrost. Université Laval, Sainte-Foy, pp. 711–717.
McColl, S.T., 2012. Paraglacial rock-slope stability. Geomorphology 153–154, 1–16.
McColl, S.T., Davies, T.R.H., 2013. Large ice-contact slope movements: glacial debuttressing, deformation and erosion. Earth Surf. Process. Landf. 38, 1102–1115.
McColl, S.T., Davies, T.R.H., McSaveney, M.J., 2012. The effect of glaciation on the intensity of seismic ground motion. Earth Surf. Process. Landf. 37, 1290–1301.
McSaveney, M., 1993. Rock avalanches of 2 may and 6 September 1992, Mount Fletcher, New Zealand. Landslide News 7, 2–4.
Mercier, D., Cossart, E., Decaulne, A., Feuillet, T., Jónsson, H.P., Sæmundsson, Þ., 2013. The Höfðahólar rock avalanche (sturzstrom): chronological constraint of paraglacial landsliding on an Icelandic hillslope. Holocene 23, 432–446.
Meunier, P., Hovius, N., Haines, A.J., 2007. Regional patterns of earthquake-triggered landslides and their relation to ground motion. Geophys. Res. Lett. 34, L20408.
Miller, D.J., Dunne, T., 1996. Topographic perturbations of regional stresses and consequent bedrock fracturing. J. Geophys. Res. 101, 25523–25536.
Mitchell, W.A., McSaveney, M.J., Zundervan, A., Kim, K., Dunning, S.A., Taylor, P.J., 2007. The Keylong Serai rock avalanche, NW Indian Himalaya: geomorphology and palaeoseismic implications. Landslides 4, 245–254.
Molnar, P., 2004. Interactions amongst topographically induced elastic stress, static fatigue, and valley incision. J. Geophys. Res. 109, F02010.
Morner, N.-A., 2004. Active faults and palaeoseismicity in Fennoscandia, especially Sweden. Primary structure and secondary effects. Tectonophysics 380, 139–157.
Morner, N.-A., 2005. An interpretation and catalogue of palaeoseismicity in Sweden. Tectonophysics 408, 265–307.
Muir-Wood, R., 2000. Deglaciation seismotectonics: a principal influence on intraplate seismogenesis at high latitudes. Quat. Sci. Rev. 19, 1399–1411.
Murphy, W., 2006. The role of topographic amplification on the initiation of rock slope failures during earthquakes. In: Evans, S.G., Mugnozza, G.S., Strom, A., Hermanns, R.L. (Eds.), Landslides from Massive Rock Slope Failure. Springer, Dordrecht, pp. 139–154.
Musson, R.M.W., 2007. British earthquakes. Proc. Geol. Assoc. 118, 305–337.
Ó Cofaigh, C., Dunlop, P., Benetti, S., 2012. Marine geophysical evidence for late Pleistocene ice sheet extent and recession off northwest Ireland. Quat. Sci. Rev. 44, 147–159.
Penna, I.M., Hermanns, R.L., Niedermann, S., Folguera, A., 2011. Multiple slope failures associated with neotectonic activity in the Southern Central Andes (37°–37°30'S), Patagonia, Argentina. Geological Soc. Am. Bull. 123, 1880–1895.
Phillips, W.M., Hall, A.M., Ballantyne, C.K., Binnie, S., Kubik, P., Freeman, S., 2008. Extent of the last ice sheet in northern Britain tested with cosmogenic ^{10}Be exposure ages. J. Quat. Sci. 23, 101–107.
Prager, C., Ivy-Ochs, S., Ostermann, M., Synal, H.-A., Patzelt, G., 2009. Geology and radiometric 14C-, 36Cl- and Th-/U-dating of the Fernpass rockslide (Tyrol, Austria). Geomorphology 103, 93–103.
Prager, C., Zangerl, C., Patzelt, G., Brandner, R., 2008. Age distribution of fossil landslides in the Tyrol (Austria) and its surrounding areas. Nat. Hazards Earth Syst. Sci. 8, 377–407.
Rasmussen, S.O., Andersen, K.K., Svensson, A.M., Steffensen, J.P., Vinther, B.M., Clausen, H.B., Siggaard-Andersen, M.L., Johnsen, S.J., Larsen, L.B., Dahl-Jensen, D., Bigler, M., Rothlisberger, R., Fischer, H., Goto-Azuma, K., Hansson, M.E., Ruth, U., 2006. A new Greenland ice core chronology for the last glacial termination. J. Geophys. Res. 111, D06102.
Ringrose, P.S., 1989a. Recent fault movement and palaeoseismicity in western Scotland. Tectonophysics 163, 305–314.
Ringrose, P.S., 1989b. Palaeoseismic (?) liquifaction event in late Quaternary lake sediments at Glen Roy, Scotland. Terra Nova 1, 57–62.
Sanchez, G., Rolland, Y., Corsini, M., Braucher, R., Bourlès, D., Arnold, M., Aumaître, G., 2010. Relationships between tectonics, slope instability and climate change: cosmic ray exposure dating of active faults, landslides and glacial surfaces in the French Alps. Geomorphology 117, 1–13.
Sellier, D., 2008. Les glissements translationnels paraglaciaires et l'évolution des grandes reliefs monoclinaux du Sutherland occidental (Highlands d'Écosse). Bull. l'Assoc. Géogr. Fr. 2, 141–152.
Seong, Y.B., Bishop, M.P., Bush, A., Clendon, P., Copland, L., Finkel, R.C., Kamp, U., Owen, L.A., Schroder, J.F., 2009. Landforms and landscape evolution in the Skardu, Shigar and Braldu valleys, Central Karakoram. Geomorphology 103, 251–267.
Shroder, J.F., Owen, L.A., Seong, Y.B., Bishop, M.P., Bush, A., Caffee, M.W., Copland, L., Finkel, R.C., Kamp, U., 2011. The role of mass movements on landscape evolution in the central Karakoram: discussion and speculation. Quat. Int. 236, 34–47.
Sigurdsson, O., Williamson, R.S., 1991. Rockslides on the terminus of 'Jökulsárgils-jökull', southern Iceland. Geogr. Ann. 73A, 129–140.
Sissons, J.B., Cornish, R., 1982. Differential glacio-isostatic uplift of crustal blocks at Glen Roy, Scotland. Quat. Res. 18, 268–288.
Soldati, M., Corsini, A., Pasuto, A., 2004. Landslides and climate change in the Italian Dolomites since the Late glacial. Catena 55, 141–161.
Stewart, I.S., Firth, C.R., Rust, D.J., Collins, P.E.F., Firth, J.A., 2001. Postglacial fault movement and palaeoseismicity in western Scotland: a reappraisal of the Kinloch Hourn fault, Kintail. J. Seismol. 6, 307–328.
Stewart, I.S., Sauber, J., Rose, J., 2000. Glacio-seismotectonics: ice sheets, crustal deformation and seismicity. Quat. Sci. Rev. 19, 1367–1389.
Stock, G.M., Uhrhammer, R.A., 2010. Catastrophic rock avalanche 3600 years BP from El Capitan, Yosemite Valley, California. Earth Surf. Process. Landf. 35, 941–951.
Stone, J.O., 2000. Air pressure and cosmogenic isotope production. J. Geophys. Res. 105 (B10), 23753–23759.
Stone, J.O., Ballantyne, C.K., Fifield, L.K., 1998. Exposure dating and validation of periglacial weathering limits, northwest Scotland. Geology 26, 587–590.
Strasser, M., Monecke, K., Schnellmann, M., Anselmetti, F.S., 2013. Lake sediments as natural seismographs: a compiled record of Late Quaternary earthquakes in Central Switzerland and its implication for Alpine deformation. Sedimentology 60, 319–341.
Van Husen, D., Ivy-Ochs, S., Alfimov, V., 2007. Mechanism and age of Late Glacial landslides in the calcareous Alps: the Almtal, Upper Austria. Aust. J. Earth Sci. 100, 114–126.
Welkner, D., Eberhardt, E., Hermanns, R.L., 2010. Hazard investigation of the Portillo Rock Avalanche site, central Andes, Chile, using an integrated field mapping and numerical modelling approach. Eng. Geol. 114, 278–297.
Wilson, P., 2009. Rockfall talus slopes and associated talus-foot features in the glaciated uplands of Great Britain and Ireland: periglacial, paraglacial or composite landforms? Geological Society, London. Special Publication 320, 133–144.
Wyrwoll, K.-H., 1977. Causes of rock-slope failure in a cold area: Labrador-Ungava. Geol. Soc. Am. Rev. Eng. Geol. 3, 59–67.
Young, N.E., Schaeffer, J.M., Briner, J.P., Goehring, B.M., 2013. A ^{10}Be production-rate calibration for the Arctic. J. Quat. Sci. 28, 515–526.